A Scanning Transmission Electron Microscopy Method for Determining Manganese Composition in Welding Fume as a Function of Primary Particle Size

Julie D. Richman[a,*,1], **Kenneth J.T. Livi**[b], and **Alison S. Geyh**[a]

[a]Johns Hopkins Bloomberg School of Public Health, Department of Environmental Health Sciences, Baltimore, MD 21205 USA (work completed at this location)

[b]Johns Hopkins University, Integrated Imaging Center HRAEM Facility, Department of Earth and Planetary Sciences and Biology, Baltimore, MD 21218 USA

Abstract

Increasing evidence suggests that the physicochemical properties of inhaled nanoparticles influence the resulting toxicokinetics and toxicodynamics. This report presents a method using scanning transmission electron microscopy (STEM) to measure the Mn content throughout the primary particle size distribution of welding fume particle samples collected on filters for application in exposure and health research. Dark field images were collected to assess the primary particle size distribution and energy-dispersive X-ray and electron energy loss spectroscopy were performed for measurement of Mn composition as a function of primary particle size. A manual method incorporating imaging software was used to measure the primary particle diameter and to select an integration region for compositional analysis within primary particles throughout the size range. To explore the variation in the developed metric, the method was applied to 10 gas metal arc welding (GMAW) fume particle samples of mild steel that were collected under a variety of conditions. The range of Mn composition by particle size was −0.10 to 0.19 %/nm, where a positive estimate indicates greater relative abundance of Mn increasing with primary particle size and a negative estimate conversely indicates decreasing Mn content with size. However, the estimate was only statistically significant ($p < 0.05$) in half of the samples (n=5), which all had a positive estimate. In the remaining samples, no significant trend was measured. Our findings indicate that the method is reproducible and that differences in the abundance of Mn by primary particle size among welding fume samples can be detected.

Keywords

welding fume; manganese; particle size distribution; primary particle; transmission electron microscopy; physicochemical property

*Corresponding author. Tel.: +1 260 685 8062; fax: +1 206 897 1991.
[1]Present Address: University of Washington School of Public Health, Department of Environmental and Occupational Health Sciences, 4225 Roosevelt Way NE, Suite 303, Seattle, WA 98105 USA

1. Introduction

Welding fume is a complex mixture of particles and gases that is highly variable. It is estimated that 90% of welding is performed with mild steel, which is composed of mostly iron (Fe) and some manganese (Mn) to strengthen the steel (Antonini, Santamaria, Jenkins, Albini, & Lucchini, 2005). In fume generated by gas metal arc welding (GMAW, or metal inert gas welding) of mild steel, previous studies have reported that the metal fraction is predominately Fe and Mn (mole fraction 77–88% and 10–23%, respectively) (Jenkins & Eagar, 2005). Fume generated by shielded metal arc welding (SMAW, or stick welding) of mild steel, contains elevated levels of elements such as silicon, potassium, and calcium, in addition to Fe and Mn (Jenkins & Eagar, 2005). Minor to trace levels of several other metals such as chromium, nickel, copper, aluminum, cadmium, magnesium, and zinc may also be present in either GMAW or SMAW of mild steel. Previous investigations of welding fume have shown that it consists of both isolated and agglomerated particles that are made up of clusters of primary particles (Farrants, Schuler, Karlsen, Reith, & Langard, 1989). The distribution of elemental content across the diameter range of the primary particles is not well understood.

Among the metals present in welding fume, Mn is of particular concern because it is a known neurotoxin. Occupational Mn inhalation exposures have been associated with the development of manganism, which is a neurological syndrome that elicits symptoms that resemble Parkinson's disease (Crossgrove & Zheng, 2004; Aschner, Erikson, & Dorman, 2005). Following inhalation, Mn can reach the brain either by transport along the olfactory nerve, via cerebrospinal fluid, or through the pulmonary system into the circulatory system (Dobson, Erikson, & Aschner, 2004). Clearance of Mn from the pulmonary system via mucocilliary transport may reduce the toxic effect on the nervous system. The relative participation of these biological pathways resulting from Mn exposure from welding fume inhalation is likely determined by particle characteristics, specifically size and Mn content.

It is well established that the size of a particle is a predictor of the site of deposition in the respiratory tract (Hinds, 1999c). However, following deposition of welding fume particles in the respiratory system, it is unclear if metal particles translocate from the respiratory tract as agglomerates or if they solubilize en route to target organs prior to elimination (Ghio & Bennett, 2007; Antonini et al., 2009). It is also possible that before elimination from the body the van der Waals and electrostatic forces holding agglomerates together are at least partially disrupted, breaking agglomerates into their primary particle constituents or smaller agglomerates, though this has not yet been thoroughly investigated. The demonstration that "aged" diesel soot agglomerates, which have been allowed time for collisional growth, can be reduced back to the fresh agglomerate size, but not smaller, by fragmenting with forced air impaction (Rothenbacher, Messerer, & Kasper, 2008), and that altered pH and presence of organic material in the fluid surrounding iron oxide nanoparticles alters their disaggregation behavior (Baalousha, 2009) suggests that multiple parameters may dictate agglomerate breakdown. With the potential for agglomerate breakdown, upon inhalation Mn content among primary particles may be associated with a physiological mechanism of clearance and interaction. In addition, the surface area would be altered with agglomerate breakdown, and in this process Mn present on the surface of primary particles may become more available for physiological interaction. Therefore, while measurements of agglomerate particle size distribution (agglomerate PSD) are determinants of the site of respiratory deposition, measuring the chemical composition throughout the primary particle size distribution (primary PSD) could be informative in understanding the resulting toxicity (Oberdörster, 1996).

Previous research indicates that Mn compositional variation in welding fume exists within agglomerates or even within primary particles (Kalliomaki, Grekula, Hagberg, & Sivonen, 1987; Voitkevich, 1988). Mn is present in welding fume predominantly in the form of magnetite (Fe_3O_4 with Mn replacing Fe to varying degrees) (Jenkins & Eagar, 2005; Minni, Gustafsson, Koponen, & Kalliomaki, 1984), though several other Mn containing compounds have been measured. Minni et al. (1990) and Kalliomaki et al. (1987) investigated composition across different types of particle configurations, including agglomerates and single particles of different sizes, using transmission electron microscopy (TEM) with energy dispersive spectroscopy (EDS) for various types of welding fume (Minni, Hofmann, & Sivonen, 1990; Kalliomaki et al., 1987). Both Minni and Kalliomaki report that the relative abundance of Mn within each sample differed among the various qualitative particle configurations, such as "granular network" and "clusters of globules", suggesting a size component to compositional difference. However, a quantitative relationship between primary particle size and composition throughout the full distribution of particle configurations present in welding fume has not been established.

The objective of this study was to develop a method utilizing electron microscopy techniques to characterize and quantify the chemical composition of the primary PSD in welding fume in a form that could readily be applied in exposure and health research. To accomplish this goal we explored the use of energy filtered transmission electron microscopy (EFTEM), and scanning TEM with electron energy-loss spectroscopy and energy dispersive (x-ray) spectroscopy (STEM/EELS/EDS) for the characterization of Mn and Fe content of primary particles ranging in size from approximately 10 to 100 nm. We applied this method to particles collected from a group of recreational welders participating in a study examining pulmonary management of inhalation exposure of Mn from welding fume. Welding fume particles were collected using a sampling method that allowed for characterization of total Mn content as well as Mn content by particle size. To characterize the agglomerate PSD relative to the estimate of primary PSD, during in a subset of welding sessions we also collected samples using a cascade impactor.

2. Methods

2.1. Particle Sample Collection

As part of a larger study examining biomarkers of exposure to welding fume, samples of welding fume were collected using personal particle samplers deployed within the breathing zone of each welder during a single welding session. Welding samples were collected under varied conditions, with welding sessions performed in different locations using different equipment and supplies. GMAW of mild steel was performed in every welding session. In one session (corresponding to sample 10), SMAW was performed in addition to GMAW. Some sessions were performed outdoors and others indoors with and without ventilation. Welding fume samples were collected over a time period that ranged from 0.65–4.45 hours.

Welding fume samples were collected using a Personal and Microenvironmental Aerosol Speciation Sampler (PMASS, MSP Corporation, Shoreview MN), which allows for simultaneous collection of duplicate particle samples. The PMASS includes a single size selective inlet and two parallel sampling channels. The inlet is an aluminum cyclone, which has a 50% cut-size of 2.5 µm at 4 L/min. The sampler operates with one pump, which pulls flow through both channels. A Teflon filter with a PTFE support ring (3.0 µm pore size, 25 mm, Pall Life Sciences, Ann Arbor MI) was placed in one PMASS channel and a polycarbonate filter (3.0 µm pore size, 25 mm, Nuclepore Track-Etched Membrane, Whatman, Kent UK) was placed in the second channel. The air flow was passively split to approximately 2 L/min through each channel. Membrane discs were placed under filters to help balance the flow. Total flow was measured using a flow meter (Drycal DC-Lite &

DC-2, BIOS, Butler NJ). The flow rate through each filter was determined by simultaneously measuring flow through each channel using side-by-side rotameters and then calculating the percent of the total flow through the entire system. To adjust for background contamination on the Teflon filter, at least one Teflon filter blank was obtained during each welding session. After collection, all samples were stored in amber glass jars under argon gas prior to sample preparation and analysis.

2.2. Electron Microscopy Method Selection

Two spectrum imaging techniques were explored for obtaining Mn and Fe compositional data for particles throughout the entire size distribution: EFTEM and STEM/EELS/EDS mapping. Although EFTEM is generally not considered to be quantitative, with EFTEM an image containing compositional information can be collected relatively quickly (within minutes) (Egerton, 1996; Moore, Elbert, & Veblen, 2001). STEM/EELS/EDS analysis required longer acquisition time, but provided greater compositional contrast and lower detection limits, especially for particles at the smaller end of the size distribution. The STEM/EELS/EDS method was selected because: 1) the STEM/EELS Mn and Fe compositional results had greater precision and sensitivity, and 2) utilizing the STEM provided more information for post data acquisition exploration because spectral data from the complete sample is stored during acquisition. Having stored spectral data over the scanned region allowed for more flexibility to investigate a specific region or composition of a sample of interest after the sample was initially analyzed. Within the STEM analysis, EELS was selected as the technique for estimating primary particle composition because it has greater sensitivity than EDS within small spatial regions (used for areas ~4nm in this study). The incorporation of EDS in tandem with EELS analysis allowed for secondary confirmation of TEM bulk estimates and for comparison to previously reported estimates from bulk EDS of welding fume. In addition, applying EDS enabled the analysis of the bulk composition of other elements of interest, such as silicon (Si).

2.3. Scanning Transmission Electron Microscopy

To determine the size and Mn composition of primary particles, dark-field (DF) intensity images, as well as EELS and EDS data were collect using a Philips CM 300 FEG S/TEM microscope operating at 297 kV (Figures 1 & 2). An Annular Dark-Field (ADF) detector was used to collect the 2D DF spatial image. A Gatan GIF 200 within the STEM was used to collect EELS spectra containing the O (oxygen) K and Mn and Fe $L_{2,3}$ core-loss edges that are separated by differences in loss in energy of the incident electrons after inelastic interaction with the atoms of the sample. A 2 mm entrance aperture of the GIF resulted in a collection angle of 15 mrad and a convergent angle of 4 mrad. EDS spectra were collected in the STEM analysis using an Oxford ultrathin window detector and an EmiSpec processor that separates elements by characteristic energy of emitted x-rays. Simultaneous collection of EELS and EDS data during acquisition was accomplished using ESVision software (version 4, FEI, Hillsboro OR). Signals from three different detectors: the GIF, EDS spectrometer, and ADF, simultaneously collected the entire EELS and EDS spectral data set and corresponding image with each pixel stored to create a data hypercube. This allowed for quantifiable compositional data from both EELS and EDS from each pixel of known location in the imaged sample.

DF images were collected at a pixel resolution of 0.3 nm (3008×2687 pixels). EELS and EDS maps were collected at pixel resolution of 5–10 nm/pixel with maps containing approximately 100×100 pixels in a smaller area than their corresponding DF images. A dwell time of 1 s per pixel resulted in total acquisition times of approximately 4 hrs for the EELS and EDS maps. Drift correction was employed during acquisition; however, since the DF images were acquired before the maps and at a different pixel resolution, some drift

between images was still possible. Therefore, residual drift was assessed visually after acquisition.

A dispersion of 0.3 eV per channel was chosen for EELS collection so that the O K (~532 eV), Mn $L_{2,3}$ (~640 eV) and Fe $L_{2,3}$ (~708 eV) core-loss edges could be collected simultaneously (Figure 1). While Mn and Fe were the elements of interest, the O K edge was included since it was the third major element and necessary for calculation of atomic percents. In addition, the O K edge contains information about individual particle crystal structures. The EELS spectra were corrected for background using a power-law function and the multiple scattering contribution (thickness effects) was removed by deconvolution with the low-loss region (Egerton, 1996). The atomic proportions of O, Mn and Fe were calculated using the Gatan Digital Micrograph version 3.8.2 software package.

2.4. Determination of Primary Particle Size Distribution

Polycarbonate filters were selected as the particle collection substrate for primary particle size and composition analysis because the particles concentrate on top of the filter and are more easily imaged in the TEM then they would be on substrates, such as Teflon filters, that entrap particles within the media. In preparation for microscopy, particle samples were washed with 100% ethanol, embedded in epon, and sectioned to approximately 80 nm thickness through the cross section of the filter using a Leica UCT ultramicrotome. The sectioned filters were then placed onto a nickel grid and carbon coated at 297 kV to reduce charging.

For each sample, a DF image was collected for particle sizing. Publicly accessible imaging software (Image J, US National Institutes of Health, Bethesda MD) designed to provide an automatic estimation of the primary PSD was initially explored as a tool for quantifying the size distribution. However, for these welding fume samples the imaging resolution was inadequate to correctly account for the majority of the primary particles (<10 nm). This was due to overlapping particles, as well as the low contrast between the smallest primary particles.

A manual method was, therefore, established using ES Vision software. A grid containing nine 250×250 nm fields was drawn on each DF image to define potential areas for particle counting (Figure 2). To determine the minimum number of fields required for providing a statistically representative sample of particles for the estimate of particle size, a series of tests were conducted. Initial tests began with counting all particles (approximately 2000 particles) in 9 fields of a single DF image followed by counting all particles per field for different subsets of fields. Based on the count median diameter estimates, it was determined that a statistically representative sample was achieved when approximately 1000 particles within 5 fields were counted.

To characterize the primary PSD, the following sizing rules were established: 1) All primary particles within 5 fields from the grid of alternating spacing were sized; 2) If 1000 particles were not sized after assessing 5 fields particles, the remaining fields of the image and additional images were sized until 1000 particles had been measured; 3) Once starting to size particles within a field, all particles within that field were sized; and 4) At least half of a particle had to be included in the field to be measured.

Individual particles were sized by overlaying a circular drawing object with the best fit by visual inspection to the particle circumference. Applying the concept of a Porton graticule, which is used for estimating the particle size distribution in optical microscopy, size bins were defined as a $\sqrt{2}$ geometric progression of the diameter (Hinds, 1999b). The size bins were determined by the equation: $d_n = d_0(2)^{n/2}$, where "d" is the diameter of the particle, "n"

is the number of the size bin with "d_0" as the smallest particle diameter. Based on a review of two representative samples with sufficient magnification to visualize the largest particles, it was determined that the smallest particle diameter that could be estimated with confidence was 4 nm. To be conservative, the smallest size bin was, therefore, defined as all particles ≤6 nm in diameter. The particle size distribution was determined by counting the number of particles that fell within each size bin, and measuring the cumulative frequency of particles throughout the size distribution. In order to determine the count median diameter (CMD), the mid-point diameter of each size bin was log transformed and then plotted against the z statistic of a standard normal distribution corresponding to the cumulative fraction of particles within the size bin (Hinds, 1999b; Moore & McCabe, 1993).

2.5. Determination of Manganese Composition by Particle Size

To characterize composition, the DF image was overlaid onto an EELS spectrum image with the corresponding composition spectrum (Figure 2). For quantification of Mn and Fe content from EELS spectra within each specified particle size bin, 10 particles were selected at random from the DF image that had previously been used for estimation of primary PSD. To be eligible for this analysis, areas free of overlap from other particles were selected as the integration area for EELS and EDS spectra. The spectra stored at every pixel within the overlap-free region of a particle were summed and processed for determination of Mn composition.

The contribution of Mn in each particle was then quantified as the percent of Fe contribution, because Fe is the most abundant metal in the samples. Mn composition per particle was reported as "the relative abundance of Mn", defined as $100* Mn/(Mn + Fe)$, where each elemental quantity is represented as an atomic fraction and the resulting unit is percent. The atomic fractions of Mn and Fe were estimated by normalizing to oxygen (i.e. Mn/O & Fe/O).

Accordingly, each selected primary particle in the welding fume sample simultaneously has an estimate of relative abundance of Mn from the EELS spectrum, as well as a measure of primary particle diameter from the DF image. An estimate of the Mn composition across the primary particle size distribution for each sample was assessed by linear regression of the relative abundance of Mn by particle vs. the particle diameter of that specific particle. The slope of this linear regression is termed the "Mn composition by particle size". A statistically significant positive slope indicates that smaller primary particles within a welding fume sample are composed of less Mn compared to larger primary particles within that sample, and a statistically significant negative slope indicates the converse. A slope that is not statistically different from zero indicates that there is no trend in Mn composition by primary particle size.

2.6. Method Validation of Size Distribution and Mn Composition by Particle Size

Four people were involved in the analysis of the STEM/EELS/EDS data sets. To validate the reproducibility of the method, each person was asked to evaluate a common data set obtained from a single sample. The results of these separate analyses were then evaluated for comparability. Between-person comparability in the assessment of primary PSD was determined by comparison of the CMD estimates. Comparability of the Mn composition across the primary PSD was evaluated by comparing slope of estimates of relative abundance of Mn vs. primary particle size.

The primary PSD of the validation sample as measured by these four people had an estimated CMD of 7.6 nm and average geometric standard deviation (GSD) of 2.5 (Table 1).

Overlap of the 95% confidence intervals of the CMD's and a chi-square test indicate that the CMD estimated between individuals were not statistically different (p=0.99).

The average Mn composition by particle size of the validation sample by the four counters was 0.21 %/nm (SD 0.06 %/nm), (Table 1). As with the primary PSD, the 95% confidence intervals overlap, and a chi-square test indicates that the composition measures were not significantly different between counters (p=0.13).

2.7. Measurement of Total Metal Content

Total Mn content was assessed using the particle sample collected on the Teflon filter. To determine total mass, all filters were weighed before and after sample collection using a Mettler T5 microbalance with precision of ± 0.003 mg (Mettler-Toledo, Columbus OH) after equilibrating for 24 hrs in a temperature and humidity controlled weighing room. All mass values of samples were blank-corrected.

In preparation for analysis of elemental mass, the polyolefin ring was removed from the Teflon filter. Samples were then digested in 74% HNO_3 (optima grade, Fisher Scientific, Columbia MD) plus ultrapure water at 150°C for 30 minutes using a microwave digestion system (MARS XPress CEM Corp., Matthews NC). At the end of the first digestion, HF (optima grade, Fisher Scientific, Columbia MD) and HNO_3 were added to achieve a final solution of 73% HNO_3 and 9% HF. Samples were then digested again under the same system conditions. Digested samples were diluted with ultrapure water to a final concentration of 2% HNO_3.

Filters were analyzed for total Mn and Fe mass by ICP-MS (Agilent 7500ce, Agilent Technologies, Newark DE). For every ten samples, at least two samples of the standard reference material SRM 2709 (NIST material 2709 San Joaquin soil; National Institute of Standards, Rockville MD) were also digested and analyzed. Samples were run against a 4–7 point calibration curve, depending on the concentration range of the samples. Scandium was used as an internal standard and sample metal concentrations were blank-corrected.

2.8. Measurement of Agglomerate Particle Size Distribution

Since it is assumed that welding fume particles are present mainly as agglomerates, the particles size distribution measured by impaction are therefore essentially a measure of the agglomerate distribution. For a subset of welding sessions, a stationary Electrical Low Pressure Impactor (ELPI, Dekati Ltd., Tampere Finland) was deployed simultaneously with the PMASS to allow for assessment of the agglomerate particle size distribution. The ELPI is a 13-stage cascade impactor that determines the number of particles collected by accumulated charge on each impaction stage. When operated at 10 L/min, the ELPI size segregated particles with diameters between 30 and 10,000 nm based on aerodynamic diameter. For this study, the intake of the ELPI was placed approximately 10 ft from the source of the welding fume. Greased aluminum substrates were used for sample collection to reduce particle bounce. Dekati instrument software was used for data analysis. The Cunningham slip correction factor was applied to account for aerodynamic properties of particles less than 1 µm in diameter. From the cumulative fraction of particles in each size-specific stage, the agglomerate CMD was determined by estimating the agglomerate size distribution.

3. Results

3.1. Particle Sample Collection

A total of 10 welding sessions were completed, resulting in 10 samples that were characterized for primary particle size and composition. The average pump flow for samples collected on Teflon filters was 2.24 L/min (range: 1.89–2.68 L/min). The average pump flow for samples collected on polycarbonate filters was 1.57 L/min, (range: 1.43 to 1.89 L/min).

3.2. Primary Particle Size Distribution

Welding fume particle sample diameters ranged from <4nm to 168 nm. The average primary particle CMD was 6.5 nm with an average GSD of 2.5 (Table 1). The estimated CMD's of the samples were statistically significantly different (chi-square test, p<0.05), indicating that welding sessions had unique primary particle size distributions.

3.3. Total Metals Analysis

Samples were analyzed in two batches for total metal concentration. Method detection limits (MDL's), measured as 3 times the standard deviation of the blank filter, for each batch were 0.6 and 0.2 µg/m^3 for Mn, and 6 and 2 µg/m^3 for Fe. The SRM recoveries were within 10% of the expected values in both batches, so no correction factors were applied.

The average mass fraction of total Mn in the welding fume samples was 6.0% (range: 0.8–10%). The average mass fraction of total Fe was 33% (range: 22–47%). The combined mass fraction of Mn and Fe in the samples was an average of 39% (range: 23–56%) (Table 2).

3.4. Characterization of Mn Composition by Particle Size

In the 10 samples, the composition and size were measured in a total of 770 primary particles. The average relative abundance of Mn for individual particles was 5.7% (range: 0–88%). The average Mn composition size slope was 0.09 %/nm (std dev 0.09) (Table 1). The Mn composition was not uniform throughout the size distribution of each sample or across samples (chi-square test, p<0.0001). (See supplemental figure for results from individual samples.) Linear regression of Mn composition by primary particle size resulted in a statistically significant positive linear slope for half of the samples (n=5) and no significant linear trend in the remaining 5 samples (Table 1).

3.5. Comparison of TEM Bulk EDS and EELS

The average bulk estimate of relative abundance of Mn measured by EDS was 12% (std dev 5%), and by EELS was 14% (std dev 5%) (Table 3). On average, the bulk estimates of Mn relative abundance determined by EDS were 11% less than those determined by EELS (range of difference: −35% to 56%).

3.6. Size Distribution of Agglomerate Particles

The agglomerate PSD was estimated from measurements collected by the ELPI during four of the welding sessions conducted under similar conditions. Data from one session was omitted due to particle overload in the ELPI, resulting in total of three reported sessions. Agglomerated particle diameters ranged from 56 to >10,030 nm with an average CMD of 105 nm and an average geometric standard deviation (GSD) of 2.7 (Table 4). (The corresponding primary particle CMD obtained via microscopy for the welding session is also presented in Table 4.) Applying the Hatche-Choate conversion to each CMD gave an average mass median diameter of 2300 nm.

4. Discussion

This research presents a method developed for characterizing the content of Mn throughout size range of primary particles in welding fume that was applied to ten samples. There was a statistically significant positive trend of increasing Mn composition with primary particle size in half of the welding fume samples. A combined analysis for Mn composition by particle size using all 10 samples resulted in an estimate that was significantly positive (0.09 %/nm, 95% CI: 0.05, 0.1) (Figure 3). The combined analysis shows that the largest primary particle has twice the relative Mn abundance as compared to the smallest primary particle.

The diameter of primary particles measured in welding fume samples ranged from 4 nm to 166 nm with the majority of particles (85%) <17 nm in diameter. Analysis of the primary PSD of the welding fume samples resulted in estimated CMD's that were all <10 nm. Though the primary particle CMD estimates in this study have a relatively small range (3.3–9.8 nm), the largest estimate of CMD was statistically different from the smallest, indicating diversity in the primary particle size distributions across samples. If the data from all 10 samples are pooled to represent a single welding fume sample, the estimated CMD is 6.0 nm (GSD 2.4). To the best of our knowledge, this is the first report of both CMD and metal composition of welding fume based on measurements of primary particles.

As exposure characterization improves, it is becoming increasingly evident that both composition and particle size of inhaled aerosols are important determinants of the resulting health outcomes. In controlled laboratory settings it is possible to generate aerosols that have homogenous characteristics of particle size and composition and to apply these particles to toxicology or controlled human exposure studies. This is useful in investigating basic principles of associated health effects. However, in non-laboratory generated aerosols, such as those present in the general environment arising from multiple sources, or complex single occupational sources such as welding, there is no reason to expect that the composition of particles is the same throughout the size distribution. To fully understand the implications of true human inhalation exposures, it will be necessary to develop more sophisticated measures that explore a range of aerosol parameters.

Toxicological research focused on engineered nanoparticles offers some insight to the importance of fully characterizing welding fume. Nanoparticles of similar chemical composition to larger particles have been shown to have higher inflammatory potential when compared on a mass per mass basis (Oberdörster, Oberdörster, & Oberdörster, 2005). Other health effects are also likely to be a greater concern for nanoparticles in contrast to larger particles. It is, therefore, not clear that defining exposure in terms of simple mass concentration is appropriate when considering exposure to particles in the nanometer size range. Several recent studies have examined differences in the explanatory power of mass concentration (the metric typically used for aerosols of larger particles), specific surface area, number concentration, agglomerate particle size or primary particle size in accounting for resulting toxicity (Limbach et al., 2005; Oberdörster et al., 2005; Tran et al., 2000; Wittmaack, 2006). In comparing toxicity of nanoparticles with differing composition, the discrepancy found in the association of these different measures of exposure may be at least partly attributed to the degree of agglomeration and ability to disaggregate, which is in turn associated with the surface chemistry and number concentration (Hinds, 1999a; Baalousha, 2009). Measuring these properties among the primary particles of the agglomerates may offer further insight.

To date, little is known about the influence of primary particles on toxicity. Oberdörster et al. (1996) report that following a 3-month inhalation exposure to similarly sized primary particles of TiO_2 (primary particle diameter ~20 nm) and carbon black (primary particle

diameter 15–50 nm), rats exposed to the TiO_2 exhibited approximately twice the lung burden in the regional lymphs as compared to carbon black (Oberdörster, 1996). Oberdörster hypothesized that the ability of the TiO_2 to translocate from the respiratory system may be due to the fact that carbon black fuses into aggregates, while TiO_2 more readily disaggregates or remains as primary particles. Pauluhn et al. (2009) report that in rats exposed to aluminum oxyhydroxide, the size of the agglomerate determined toxicity, while the size of the primary particle determined the clearance rate (Pauluhn, 2009). This suggests that both physical and chemical properties can alter the physiological interaction in complex ways. As such, a combination of particle metrics for interpretation of different outcome parameters may be useful.

Based on interpretation of the results obtained for the metrics developed in this study for welding fume samples, we hypothesize that the following toxicokinetics would occur upon inhalation. The average estimated agglomerate CMD of 105 nm, which is approximately 16 times larger than the average primary particle CMD, suggests that the site of respiratory deposition following inhalation would be predominantly in the alveolar region (Hinds, 1999c). In the alveolar region there is less opportunity for rapid clearance, and greater potential for uptake into the circulatory system compared to the upper airways. Smaller fractions of the welding fume would deposit in the head airways and tracheobronchial regions where mucociliary clearance occurs (Hinds, 1999c). After deposition, should the agglomerates disaggregate, the results reported by Oberdörster and Pauluhn suggest that the primary particles would translocate further and with slower clearance rates than intact agglomerate particles (Oberdörster, 1996; Pauluhn, 2009). Extrapolating from our estimate of a trend in Mn composition by primary particle size, the smallest isolated primary particles with the slowest clearance rates would have less Mn content.

Adding to this interpretation, Hewett investigated welding fume Mn and Fe composition by the assumed agglomerate particle size. Hewett reports that the size segregated Mn and Fe content from SMAW and GMAW fume collected by the MOUDI "appear similar" across the size distribution, but noted that this was only based on a single sample of each type of fume (Hewett, 1995). If the agglomerates do not disaggregate following deposition, this suggests there may not be a differential effect of varying Mn content in the primary particles in welding fume unless "hot spots" of greater Mn concentration on the agglomerate surface are important in understanding the physiological interaction. In contrast, if the agglomerates disaggregate, variation of Mn content throughout the primary PSD rather than the agglomerate PSD may be a determinant of the resulting physiological effect. Further research will be required to establish this association.

As a means of evaluating the measurement of Mn composition by primary particle size, a comparison of the estimates of relative abundance of Mn by EELS vs. EDS shows the two methods to be in good agreement (on average within 11%). The relative abundance of Mn estimated in this investigation ranged from 4–22% from EELS, and 3–18% from EDS analysis. Based on data reported by Minni et al., Kalliomaki et al., and Jenkins & Eager from bulk EDS analysis of GMAW of mild steel, we calculated a relative abundance of Mn ranging from 1– 35%, 8–20%, and 10% respectively (Jenkins & Eagar, 2005; Minni et al., 1990; Kalliomaki et al., 1987), which is consistent with our results.

Obtaining bulk EDS estimates also provided the opportunity to investigate the relative abundance of Si, defined as: $Si/(Si + Mn + Fe)$, where each element is estimated as an atomic fraction. The average relative abundance of Si was 15% (range: <1%–42). While Mn is known to be present in iron oxides in welding fume, Si can also substitute into the Mn-Fe-oxide structure. If Si is present, it may alter the solubility and oxidation state of the Mn phase, which may alter the physiological interaction of Mn. A more in depth study of the

various compounds of Mn present throughout the size distribution and variation among welding fume samples could further inform this distinction.

Limitations

This method was developed specifically for welding fume, which is comprised of spherical primary particles. The ability to use a circular shape tool within the imaging software to characterize primary particle size greatly simplified the method. Different and more complicated shape tools would be necessary for particles that were not spherical.

The wide confidence intervals of the Mn composition by particle size estimates are likely to be due both to a true spread of Mn compositions by particle size and to the fact that only 63–88 particles per sample were selected to be analyzed for compositional analysis (depending on the range of diameters in the size distribution of each sample). Assessment of a test sample confirms that analyzing more particles would have improved the statistical confidence in the measure. In the test sample, composition was measured with the number of particles defined by the protocol and then with double that the number of particles; the confidence intervals obtained from analysis with twice the number of particles were nearly half as wide as those estimated with fewer particles (data not shown). The determination of the number of primary particles to analyze for composition was based, in part, on feasibility. As such, a limitation of estimating the Mn composition by particle size slope is the time required to analyze each particle.

By the design of this study it is not possible to determine if the unique measurements of primary PSD and Mn composition by particle size were due to different conditions that generate welding fume, though it is known that several factors lead to differences in the fume. For example, Mn content varies among the welding rod or wires (Voitkevich, 1988). Furthermore, GMAW, which was performed in the generation of all of the samples presented here, is associated with a smaller agglomerate PSD than shielded metal arc welding (mass median aerodynamic diameter 240 nm vs. 590 nm, respectively) (Hewett, 1995). Welding technique also appears to be an important determinant in the size distribution. Research conducted by Zimmer et al. has shown that when compared, welding fume automatically generated with the same equipment and materials, but with the equipment operated in two different modes ("globular transfer" vs. a "spray transfer"), the agglomerate geometric mean particle diameter was larger for globular transfer (113 nm vs. 89 nm) (Zimmer, Baron, & Biswas, 2002).

5. Conclusion

The data processing method described here provides two measures of exposure characterization that contribute to the understanding of exposures: a measure of primary particle size distribution, and a measure that incorporates the particle composition throughout the size distribution. These two forms of particle characterization are presented as metrics that can easily be interpreted and applied to exposure assessment studies. While this method is labor intensive, it is found here to be reproducible. In addition, in the small sample set investigated, estimates of both primary particle size and Mn composition by particle size were found to vary significantly. Further research will be required to investigate the conditions in welding fume generation that contribute to different measurements of primary particle CMD or Mn composition by particle size and to determine the association between different health effects associated with these exposures. Application of the measurement of Mn composition by particle size in exposure assessment studies will contribute to the body of research that simultaneously characterizes particle size and composition. Ultimately, these measures of physical and chemical properties will improve our understanding of the resulting toxicity of welding fume and inhalation of metals.

Supplementary Material

Refer to Web version on PubMed Central for supplementary material.

Acknowledgments

Reference List

Antonini JM, Santamaria AB, Jenkins NT, Albini E, Lucchini R. Fate of manganese associated with the inhalation of welding fumes: Potential neurological effects. Neurotoxicology. 2005; 27

Antonini JM, Sriram K, Benkovic SA, Roberts JR, Stone S, Chen BT, et al. Mild steel welding fume causes manganese accumulation and subtle neuroinflammatory changes but not overt neuronal damage in discrete brain regions of rats after short-term inhalation exposure. Neurotoxicology. 2009; 30:915–925. [PubMed: 19782702]

Aschner M, Erikson KM, Dorman DC. Manganese dosimetry: species differences and implications for neurotoxicity. Crit Rev.Toxicol. 2005; 35:1–32. [PubMed: 15742901]

Baalousha M. Aggregation and disaggregation of iron oxide nanoparticles: Influence of particle concentration, pH and natural organic matter. Science of The Total Environment. 2009; 407:2093–2101. [PubMed: 19059631]

Crossgrove J, Zheng W. Manganese toxicity upon overexposure. NMR Biomed. 2004; 17:544–553. [PubMed: 15617053]

Dobson AW, Erikson KM, Aschner M. Manganese neurotoxicity. Ann.N.Y.Acad.Sci. 2004; 1012:115–128. [PubMed: 15105259]

Egerton, RF. Electron Energy Loss Spectroscopy in the Electron Microscope. 2nd ed.. New York: Plenum Press; 1996.

Farrants G, Schuler B, Karlsen J, Reith A, Langard S. Characterization of the morphological properties of welding fume particles by transmission electron microscopy and digital image analysis. Am.Ind.Hyg.Assoc.J. 1989; 50:473–479. [PubMed: 2801515]

Ghio AJ, Bennett WD. Metal particles are inappropriate for testing a postulate of extrapulmonary transport. Environ.Health Perspect. 2007; 115:A70–A71. [PubMed: 17384740]

Hewett P. The particle size distribution, density, and specific surface area of welding fumes from SMAW and GMAW mild and stainless steel consumables. Am.Ind.Hyg.Assoc.J. 1995; 56:128–135. [PubMed: 7856513]

Hinds, WC. Aerosol Technology. Second ed.. New York: John Wiley & Sons, Inc.; 1999b. Microscopy Measurement of Particle Size; p. 402-427.

Hinds, WC. Aerosol Technology. second ed.. New York: John Wiley & Sons, Inc.; 1999c. Respiratory Deposition; p. 233-259.

Hinds, WC. Aerosol Technology. second ed.. New York: John Wiley & Sons, Inc.; 1999a. Adhesion of Particles; p. 141-149.

Jenkins NT, Eagar TW. Chemical Analysis of Welding Fume Particles. Welding Journal. 2005:87-s–93-s.

Kalliomaki PL, Grekula A, Hagberg J, Sivonen S. Analytical electron microscopy of welding fumes. Journal of Aerosol Science. 1987; 18:781–784.

Limbach LK, Li Y, Grass RN, Brunner TJ, Hintermann MA, Muller M, et al. Oxide Nanoparticle Uptake in Human Lung Fibroblasts:ГÇë Effects of Particle Size, Agglomeration, and Diffusion at Low Concentrations. Environmental Science & Technology. 2005; 39:9370–9376. [PubMed: 16382966]

Minni E, Hofmann S, Sivonen SJ. An AES study of particles in welding fumes of mild and stainless steel. Surface and interface analysis. 1990; 16:563–564.

Minni E, Gustafsson TE, Koponen M, Kalliomaki PL. A study of the chemical structure of particles in the welding fumes of mild and stainless steel. J.Aerosol Sci. 1984; 15:57–68.

Moore, DS.; McCabe, GP. Introduction to the Practice of Statistics. Second ed.. New York: W.H. Freeman and Company; 1993. Looking at the Data: Distributions; p. 3-35.

Moore KT, Elbert DC, Veblen DR. Energy-filtered transmission electron microscopy (EFTEM) of intergrown pyroxenes. American Mineralogist. 2001; 86:814–825.

Oberdörster G. Significance of particle parameters in the evaluation of exposure-dose-response relationships of inhaled particles. Inhal.Toxicol. 1996; 8 Suppl:73–89. [PubMed: 11542496]

Oberdörster G, Oberdörster E, Oberdörster J. Nanotoxicology: an emerging discipline evolving from studies of ultrafine particles. Environ.Health Perspect. 2005; 113:823–839. [PubMed: 16002369]

Pauluhn J. Pulmonary Toxicity and Fate of Agglomerated 10 and 40 nm Aluminum Oxyhydroxides following 4-Week Inhalation Exposure of Rats: Toxic Effects are Determined by Agglomerated, not Primary Particle Size. Toxicological Sciences. 2009; 109:152–167. [PubMed: 19251949]

Rothenbacher S, Messerer A, Kasper G. Fragmentation and bond strength of airborne diesel soot agglomerates. Part Fibre.Toxicol. 2008; 5:9. [PubMed: 18533015]

Tran CL, Buchanan D, Cullen RT, Searl A, Jones AD, Donaldson K. Inhalation of poorly soluble particles. II. Influence Of particle surface area on inflammation and clearance. Inhal.Toxicol. 2000; 12:1113–1126. [PubMed: 11114784]

Voitkevich VG. Investigation of heterogeneity of welding fume particle composition by the method of X-ray photoelectron spectroscopy. Soudage dans le monde [Welding in the world]. 1988; 26:108–111.

Wittmaack K. In Search of the Most Relevant Parameter for Quantifying Lung Inflammatory Response to Nanoparticle Exposure: Particle Number, Surface Area, or What? Environ Health Perspect. 2006; 115

Zimmer AT, Baron PA, Biswas P. The influence of operating parameters on number-weighted aerosol size distribution generated from a gas metal arc welding process. Journal of Aerosol Science. 2002; 33:519–531.

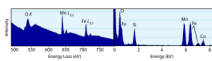**Figure 1.**
Microscopy spectra of a single particle with labeled O, Mn, and Fe peaks. Data obtained from the integration region within the square object within the left image of Figure 2. Left: STEM/EELS spectrum. Right: STEM/EDS spectrum.
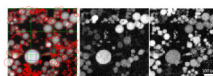
Figure 2.
TEM images of welding fume particles. Images left to right: dark field image of welding fume with applied gridlines and mapped circles, STEM/EELS Mn map, and STEM/EELS Fe map. (All images are from the same location of a sample. Brighter white on the elemental maps is associated with more abundance of the specified element.)
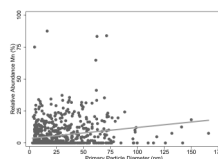
Figure 3.
Mn composition by particle size. The linear regression slope is statistically significantly positive (p<0.05).

Table 1

Primary particle size distribution and Mn composition by size of estimates: (a) analysis of a single sample by 4 people, and (b) analysis of full set of samples.

ID	Primary Particle Size Distribution				Mn Composition by Particle Size		
	Area Counted	Particles Sized	CMD	GSD[b]	Particles Quantified	Slope	Intercept
	(μm²)	(#)	(nm)[a]		(#)	(%/nm)[a]	(%/nm)[a]
a. Method Validation							
Counter							
A	0.625	1005	7.1 [5.8–8.7]	2.4	160	0.25 [0.18, 0.32]	10.7 [8.0, 13.6]
B	0.625	1072	8.0 [6.9–9.3]	2.4	90	0.13 [0.02, 0.23]	16.5 [11.2, 21.9]
C	0.375	1050	8.2 [7.3–9.2]	2.5	96	0.20 [0.11, 0.29]	16.4 [11.8, 21.1]
D	0.563	1014	7.0 [6.2–7.9]	2.7	99	0.25 [0.16, 0.35]	13.5 [9.1, 17.9]
Average:	0.547	1035	7.6	2.5	111	0.21	14.3
Std Dev:	0.118	31	0.6		33	0.06	2.8
b. Collected Samples							
Sample							
1	0.313	1474	5.0 [4.4–5.6]	2.3	67	0.10 [−0.02, 0.21]	2.0 [−0.7, 4.6]
2	0.500	1000	3.9 [3.3–4.5]	3.0	68	0.21 [0.07, 0.35]	1.4 [2.3, 5.0]
3	0.313	1209	3.2 [2.9–3.4]	2.8	72	−0.10 [−0.21, 0.01]	11.3 [8.4, 14.3]
4	0.563	1000	8.3 [7.2–9.5]	2.3	88	0.09 [0.02, 0.16]	2.4 [−0.2, 5.1]
5	0.375	1036	8.3 [7.3–9.5]	2.2	76	0.19 [0.05, 0.32]	7.6 [3.3, 11.8]
6	0.375	994	6.1 [4.7–7.9]	2.1	76	0.10 [0.04, 0.17]	−1.2 [−3.4, 10.6]
7	0.375	1162	3.3 [2.8–3.8]	2.8	70	0.10 [−0.003, 0.20]	2.1 [−0.7, 4.9]
8	1.250	1087	7.5 [6.4–8.8]	2.5	82	−0.01 [−0.04, 0.01]	1.8 [0.7, 2.9]
9	0.500	1151	9.8 [9.0–10.5]	2.1	87	0.16 [0.05, 0.26]	4.5 [−0.04, 9.0]
10	0.688	1169	9.3 [7.2–12.0]	2.1	63	0.08 [−0.15, 0.18]	2.1 [−1.9, 6.1]
Average:	0.525	1128	6.5	2.4		0.09	3.4
Std Dev:	0.281	145	2.5			0.09	3.6

[a] Estimate [95% Confidence Interval]

[b] GSD: Geometric Standard Deviation $(d_{84\%}/d_{16\%})^{1/2}$

Table 2

Total particle, Mn and Fe mass concentration in welding fume samples.

Sample	Total particle	Mn		Fe	
	Conc. ($\mu g/m^3$)	Conc. ($\mu g/m^3$)	Fraction[a] (%)	Conc. ($\mu g/m^3$)	Fraction[a] (%)
1	1251	126	10	475	38
2	8467	359	4	1981	23
3	18699	1619	9	8816	47
4	9110	681	7	4242	47
5	9497	576	6	2994	32
6	648	5	1	187	29
7	639	30	5	148	23
8	503	4	1	113	23
9	9252	808	9	4111	44
10	534	31	6	119	22
Average:	5860	424	6	2319	33
Std Dev:	6143	518	3	2829	10

[a]The fractional Mn or Fe content relative to the total particulate matter mass of the sample.

Table 3

Comparison of TEM bulk estimation of Relative Abundance of Mn.

Sample	Relative Abundance Mn		
	EELS Atomic %	EDS Atomic %	EDS vs. EELS % Difference
1	12	12	7
2	17	18	−5
3	11	9	21
4	10	13	−35
5	11	12	−11
6	4	3	30
7	22	12	44
8	16	7	56
9	18	18	2
10	13	12	8
Average:	14	12	11
Std Dev:	5	5	27

Table 4

Agglomerate and primary particle size distributions.

Sample[a]	Agglomerate PSD		Primary PSD	
	CMD (nm)	GSD	CMD (nm)	GSD
3	125	2.9	3.2	2.8
4	101	2.6	8.3	2.3
5	88	2.7	8.3	2.2
Average:	105	2.7	6.6	2.4
Std Dev:	19	0.2	3.0	0.3

[a] Agglomerate and primary PSD results with the same sample number were collected during the same welding session.